

OPEN

Experimental solubility of aripiprazole in supercritical carbon dioxide and modeling

Eslem Ansari¹, Bizhan Honarvar^{1✉}, Seyed Ali Sajadian^{2,3}, Zahra Arab Aboosadi¹ & Mehdi Azizi¹

The solubility of compounds in supercritical carbon dioxide (SC-CO₂) has found crucial significance in the fabrication of micro/nano-scaled drugs. In this research, the solubility of Aripiprazole was measured in SC-CO₂ at various temperatures (308–338 K) and pressures (12–30 MPa). Moreover, the experimental solubility results were correlated with several semi-empirical models (Chrastil, Bartle et al., Kumar & Johnston, Menden-Santiago & Teja, Sodeifian et al., and Jouyban et al.) as well as the modified Wilson model. The molar fraction of the drug in SC-CO₂ varied in the range of 1.830×10^{-6} to 1.036×10^{-5} . The solubility highly depended on the operating pressure and temperature. The Chrastil (0.994), Jouyban et al. (0.993) and Sodeifian et al. (0.992) models showed the highest consistency with the obtained values. Furthermore, self-consistency tests were performed on the solubility of Aripiprazole in SC-CO₂. The approximate total enthalpy (ΔH_{total}), vaporization enthalpy (ΔH_{vap}), and solubility enthalpy (ΔH_{sol}) were also calculated.

List of symbols

AARD%	Percent AARD, Eq. (5), (Table 4)
M_{CO_2}	CO ₂ molecular weight, Eq. (3)
M_S	Solute molecular weight, Eq. (2)
MST	Mendez-Santiago–Teja
n_{CO_2}	Mole of CO ₂ , Eqs. (1), and (3)
n_{Solute}	Mole of solute, Eqs. (1), and (2)
P_c	Critical pressure, (Table 1)
P_{sub}	Sublimation pressure (bar), (Table 1)
R	Gas constant universal (J.(mol K) ⁻¹)
R_{adj}	Adjusted correlation coefficient, Eq. (6)
S	Solubility in equilibrium state (g.L ⁻¹), Eqs. (4)–(5)
T	Temperature (K)
T_m	Melting point (K), (Table 1)
T_b	Boiling point (K), (Table 1)
T_C	Critical temperature (K), (Table 1)
V_S	Solid molar volume (m ³ .mol ⁻¹), (Table 1)
VdW2	Two-parameter Van der Waals mixing rule
V_I (L)	Sampling vial (L), Eq. (3)
V_S (L)	Represent the volume (L), Eq. (2)
S	Solubility in equilibrium state, Eq. (4)
$a_2 a_0$	Parameter, (Tables 3, 4)
$a_0 - a_5$	Parameter, (Tables 3, 4)
ΔH_2^f	Enthalpy of fusion
ΔH_{SOL}	Solubility enthalpy, (Table 5)
ΔH_{vap}	Vaporization enthalpy, (Table 5)
ΔH_t	Total heat, (Table 5)
γ_2^∞	Infinite dilution, Eq. (7)

¹Department of Chemical Engineering, Marvdasht Branch, Islamic Azad University, Marvdasht, Iran. ²Department of Chemical Engineering, Faculty of Engineering, University of Kashan, Kashan 87317-53153, Iran. ³South Zagros Oil and Gas Production, National Iranian Oil Company, Shiraz 7135717991, Iran. ✉email: honarvar2@gmail.com

$\alpha, \beta, \lambda_{12}, \lambda_{21}$ Parameters of the modified Wilson model, Eqs. (9, 10, 13), (Table 6)
 y_2 Mole fraction, Eq. (1)

Greek symbols

γ Mole fraction
 ρ Density ($\text{kg}\cdot\text{m}^{-3}$)
 ω Acentric factor

Subscripts

i, j Component
 2 Solute

Superscripts

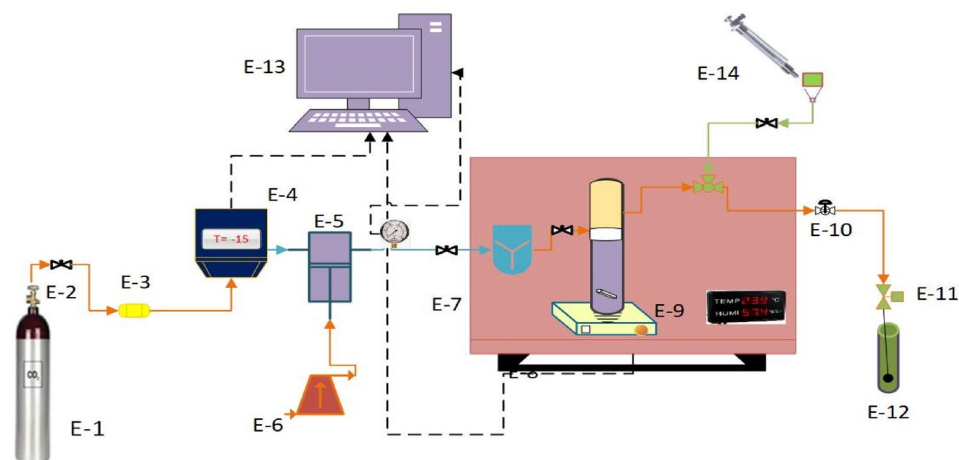
cal Calculated
 exp Experimental
 s Solute

Aripiprazole (APZ) is a second-generation antipsychotic, known as a typical antipsychotic. This drug is effective in a wide range of psychotic disorders such as schizophrenia¹. It can also serve as a mood stabilizer in the treatment of bipolar disorder^{2–4}. APZ has been approved by the Food and Drug Administration (FDA) for the treatment of mixed episodes associated with bipolar disorder and acute manic. It appears that functional selectivity at D_2 receptors may contribute to the antipsychotic effects of APZ^{5–7}. As a typical antipsychotic compound, APZ selectively binds targeting serotonin and central dopamine D_2 receptors which can be effective in the treatment of cognitive and negative symptoms of schizophrenia^{1,7}. Based on previous studies, APZ can prevent the activation of microglia by reducing the inflammatory cytokines^{8–10}. APZ can be used in the treatment of depression due to its effect on microglia activities and anti-inflammatory behavior. However, low bioavailability of Aripiprazole due to its poor aqueous solubility has significantly limited the development of APZ-based drugs and their therapeutic effects on depression^{8,11}.

Drugs with poor water solubility often show poor oral bioavailability and limited absorption rate. The improvement of the absorption, solubility, and permeability of poorly water-soluble drugs is one of the major research topics¹². The dissolution rate of the pharmaceutical compounds increases by decline of their particle size. Several conventional methods such as grinding, sieving, spray drying, and re-crystallization can be used to reduce the particle size. Each of these methods has their own drawbacks. In the last decade, supercritical fluids (SCF) technology has been employed as a micronization process to serve as an alternative to traditional methods. Researchers have used supercritical fluids as solvent or anti-solvent in the extraction processes, solution-enhanced dispersion, and solutions/suspensions rapid expansion methods^{13–22}. In addition to its moderate critical point (304.1 K as temperature and 7.38 MPa as pressure), SC- CO_2 enjoys non-polluting nature, non-flammability, non-explosiveness, and accessibility in high purity^{15,23–26}. In the process of nanoparticle production, the drug solubility in supercritical fluid is the main parameter as it determines the feasibility of supercritical methods. This parameter also specifies the role of SCF as solvent, anti-solvent, or reaction medium^{27,28}. The RESS-based processes are generally employed to prepare nanoparticle drugs with high SC- CO_2 solubility, in contrast, anti-solvent procedures are suitable in the preparation of the drug with low solubility^{29–32}. A wide range of drugs with different SC- CO_2 solubility levels have been recently examined^{25,33–35}. Moreover, various approaches have been developed to measure the drug solubility in SC- CO_2 , among which, gravimetric^{36–39}, spectrometric^{40–42}, chromatographic^{43,44}, and miscellaneous⁴⁶ methods can be mentioned. Modeling methods can also help to investigate the solubility of pharmaceuticals in SC- CO_2 with far lower time and costs and no need for complex equipment¹³.

Various mathematical models have been developed to assess the solubility of different compounds in SC- CO_2 . These methods can be categorized into several groups including equation of state (EoS), empirical and semi-empirical models, expanded liquid models, square support vector machine (LS-SVM), and artificial neural network (ANN) techniques^{45,47}. Empirical and semi-empirical models are capable of correlating the experimental solubility data to operating conditions such as temperature, pressure, and the ratio of the cosolvents to the supercritical solvent density. No need for pure solid properties is the greatest advantage of these models^{23,46,47}. The EoS are classified into two categories: cubic EoS, such as the Peng-Robinson (PR)⁵⁰ and the Soave-Redlich-Kowang (SRK)⁵¹, and non-cubic EoS. Activity coefficient-based models like modified Wilson models and universal quasi-chemical models (UNIQUAC) can be used to correlate the solubility data. The physicochemical properties of solid solutes are required in both EoS-based and activity coefficient models whose experimental measurement is a challenging and complex task. Therefore, some methods have been developed to determine the properties of solute molecules⁴⁸. Empirical and semi-empirical models (Chrastil⁴⁹, Bartle et al.⁴⁶, Kumar and Johnston (K-J)⁵³, Garlapati et al.⁵⁴, Menden-Santiago & Teja (MST)⁵⁵, Sodeifian et al.³³, Jouyban et al.⁵⁶) and expanded liquid models (universal quasi-chemical, modified Wilson's model)^{50,51} have been utilized to determine the solubility of various drugs in SC- CO_2 .

In this study, the APZ solubility in SC- CO_2 was experimentally assessed at various pressures (12–30 MPa) and temperatures (308–338 K). The results were correlated with several models including Chrastil, Bartle et al. (K-J), MST, Sodeifian et al. Jouyban et al. and modified Wilson's model. The accuracy of these models in the correlation



Equipment list					
Displayed Text	Description	Material	Displayed Text	Description	Material
E-1	CO ₂ cylinder	CO ₂	E-8	Oven	
E-2	Valve		E-9	Equilibrium Cell	CO ₂ + APZ
E-3	Filter	CO ₂	E-10	Back Pressure Valve	
E-4	Refrigerator unit	CO ₂	E-11	Metering Valve	
E-5	High Pressure Pump	CO ₂	E-12	Collection Vial	Methanol
E-6	Air compressor	Air	E-13	Control Panel	
E-7	Needle Valve		E-14	Syringe	Methanol

Figure 1. Schematic diagram of the SC-CO₂ solubility measurement used in this research.

of APZ solubility was explored by calculating and comparing average absolute relative deviation (AARD %) and adjusted correlation coefficient (R_{adj}).

Materials and methods

Materials. A sample of APZ (form II) with CAS number of 9-12-129722 and purity of 99% was purchased from Tofigh Daru Pharmaceutical Company (Tehran, Iran). Carbon dioxide (CAS number 124-38-9) with a purity of 99.98% was also supplied from Oxygen Novin Company (Shiraz, Iran). Methanol (CAS number 67-56-1) with minimum purity of 99.9% was also provided from Merck (Germany).

Physical and critical characteristics. The solubility of APZ in SC-CO₂ was quantified by thermodynamic investigations using appropriate group participation methods. The melting point (T_m) was determined by DSC analysis while the boiling point (T_b), critical pressure (P_c), and critical temperature (T_c) were evaluated by the Marrero and Gani contribution method⁵⁹. To calculate these features, the molecular structure of APZ was broke down to 10CH₂, 6CH (cyclic), 2C (cyclic), 2C-CL (cyclic), 2N (cyclic), 1C-O (cyclic), 1C-NH (cyclic), 1C, and 1O (cyclic). The molar volume (V_S) and Grain Watson⁵², sublimation pressure (P_S), and the corresponding modes of Ambrose-Walton⁵³ factor (ω) were determined according to the Immirzi-Perini method⁵⁴, as listed in Table 1.

Experimental setup and solubility assessment. The experimental setup of this device includes a CO₂ cylinder (E-1), valve (E-2), filter (E-3), refrigeration unit (E-4), high-pressure pump (E-5), air compressor (E-6), Needle valve (E-7), oven (Memmert) (E-8), equilibrium cell (E-9), back pressure valve (E-10), metering valve (E-11), collection vial (E-12), control panel (E-13), syringe (E-14), digital pressure transmitter (WIKA, Germany, code IS-0-3-2111), pressure gauge (WIKA, Germany, code EN 837-1), a digital thermometer, and 1.8-inch pipe and fittings (Fig. 1).

The high-pressure system was made of stainless steel 316. In a typical process, CO₂ first passed through a 1 μ m filter to be purified on its way to the refrigerator, at which, its temperature was reduced to -15 °C for liquefaction. The pressure of liquid CO₂ was then increased up to 12–30 MPa. Such a high pressure can be controlled through a reciprocating pump. APZ (1 g) and liquid CO₂ were then mixed and homogenized by a magnetic stirrer (100 rpm) in a cell placed in an oven for 120 min. The static time, drug content, and purity were checked by some preliminary tests. At the end of the static time, 600 μ L of saturated SC-CO₂ was loaded into the injection

Temperature (K) ^a	Pressure (MPa) ^a	Density (kg.m ⁻³) ^b	Y ₂ × 10 ⁵ (Mole Fraction)	Standard deviation of the mean, SD(\bar{y}) × (10 ⁵)	Expanded uncertainty × 10 ⁶	S × 10 (Solubility (g.L ⁻¹))
308	12	768.42	0.303	0.015	0.306	0.237
	15	816.06	0.391	0.026	0.526	0.325
	18	848.87	0.467	0.022	0.450	0.404
	21	874.4	0.513	0.034	0.688	0.457
	24	895.54	0.569	0.050	1.007	0.520
	27	913.69	0.634	0.064	1.287	0.591
	30	929.68	0.679	0.079	1.586	0.644
318	12	659.73	0.262	0.012	0.246	0.176
	15	743.17	0.357	0.023	0.466	0.270
	18	790.18	0.471	0.031	0.627	0.379
	21	823.7	0.573	0.050	1.007	0.481
	24	850.1	0.675	0.079	1.586	0.585
	27	872.04	0.741	0.072	1.448	0.659
	30	890.92	0.801	0.090	1.807	0.727
328	12	506.85	0.231	0.007	0.148	0.119
	15	654.94	0.304	0.021	0.425	0.203
	18	724.13	0.496	0.025	0.510	0.366
	21	768.74	0.643	0.048	0.969	0.504
	24	801.92	0.759	0.073	1.468	0.620
	27	828.51	0.847	0.086	1.729	0.716
	30	850.83	0.913	0.077	1.551	0.792
338	12	384.17	0.183	0.006	0.126	0.072
	15	555.23	0.258	0.017	0.344	0.146
	18	651.18	0.499	0.043	0.866	0.331
	21	709.69	0.699	0.056	1.129	0.506
	24	751.17	0.877	0.078	1.570	0.671
	27	783.29	0.958	0.095	1.910	0.764
	30	809.58	1.036	0.120	2.409	0.855

Table 2. The APZ solubility at distinctive operational conditions (12–30 MPa) and (308–338 K). The experimental standard deviation of the mean (SD) were obtained by $SD(\bar{y}) = \frac{s(y_k)}{\sqrt{n}}$. n is the number of times each experimental data was measured ($n = 3$, in this work). Expanded uncertainty is $U = k \cdot u_{combined}$ and the relative combined standard uncertainty is defined as $u_{combined}/y = \sqrt{\sum_{i=1}^N (P_i u(x_i)/x_i)^2}$ in which $u(x_i)/x_i$ is the relative standard uncertainty of each input estimate (x_i) and P_i is known positive or negative number having negligible uncertainties. ^aStandard uncertainty u are $u(T) = 0.1$ K; $u(p) = 1$ bar. Also, the relative standard uncertainties are obtained below 0.05 for mole fractions and solubility's. The value of the coverage factor $k = 2$ was chosen on the basis of the level of confidence of approximately 95 percent. Data from the Span–Wagner equation of state.

loop through a three-valve two-position valve. By opening the injection valve, the sample collected inside the vial was released with 5 ml of methanol which had been already loaded. Subsequently, the vial was washed by the syringe pump which injected 1 ml of methanol. The drug content of the obtained sample was evaluated by a spectrophotometer at a wavelength of 254 nm. A calibration curve was also used to estimate the concentration of the solutes. A set of standard solutions were obtained through diluting the stock solutions. Drug solubility in SC-CO₂ can be calculated at various pressures and temperatures using the following equations:

$$y_2 = \frac{n_{solute}}{n_{solute} + n_{CO_2}} \quad (1)$$

$$n_{solute} = \frac{C_s \times V_s}{M_s}, \text{ and} \quad (2)$$

$$n_{CO_2} = \frac{V_1 \times \rho}{M_{CO_2}}, \quad (3)$$

where n_{solute} and n_{CO_2} denote the number of moles of the solute and CO₂, respectively, C_s shows the solute concentration (g.L⁻¹) based on the calibration curve. $V_s(L)$ and $V_1(L)$ represent the volumes of the sampling vial

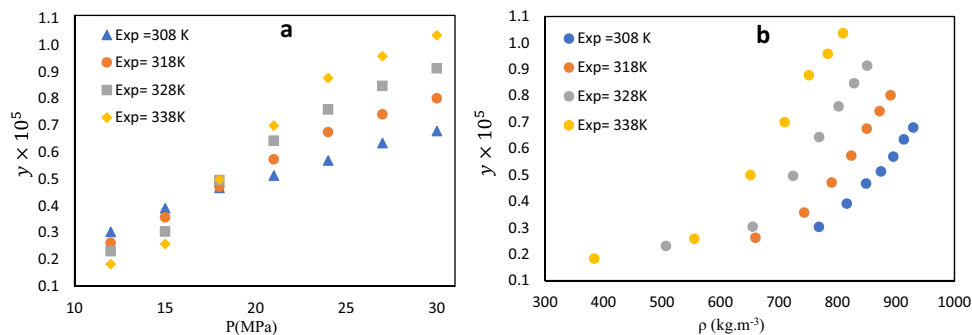


Figure 2. Experimental solubility of APZ in SC-CO₂ at various pressures and temperatures. **(a)** Solubility according to pressure and **(b)** solubility according to density.

and collection ring, respectively. M_S and M_{CO_2} stand for the molecular mass of the solute and CO₂, respectively. Equation (4) expresses the equilibrium solubility of the solute (S) in SC-CO₂:

$$S = \frac{\rho \times M_{\text{solute}} \times y_2}{M_{CO_2} \times (1 - y_2)}. \quad (4)$$

Results and discussion

Experimental data. The solubility of APZ in SC-CO₂ was examined at different temperatures (308–338 K) and pressures (12–30 MPa). The measurements were carried out in triplicates to reduce the error. Data of APZ solubility in SC-CO₂ including its mole fraction (y), density (ρ), solubility (S), and expanded uncertainty are also presented in Table 2. Accordingly, the highest APZ mole fraction (1.036×10^{-5}) was detected at 338 K and 30 MPa whereas the lowest value (1.830×10^{-6}) was recorded at 338 K and 12 MPa. The solubility showed an ascending trend with increasing the pressure at high temperatures. As the pressure rises, the density of SC-CO₂ increases which enhances the strength of the solvent. The solvent density and the vapor pressure of the solution are the main factors in the solubility enhancement. Based on Fig. 2, the solubility curve showed a crossover region. Temperature generally exhibited a dual effect on drug solubility in SC-CO₂ under controlled SC-CO₂ density and drug vapor pressure. The solubility of APZ in SC-CO₂ decremented in the pressure range of 12–18 MPa by enhancing the temperature. At pressures above 18 MPa, the solubility rose with temperature elevation. The crossover region for APZ ranged from 12 to 18 MPa. At pressures lower than 18 MPa, the effect of density was predominant as the solubility increased by temperature reduction. However, at pressures above 18 MPa, solubility rose with temperature increment due to the predominance of the influence of the vapor pressure of the drug. The impact of temperature on carbon dioxide density and vapor pressure of solute was reported by several articles with similar values of the SC-CO₂ pressure crossover region for Nystatin⁵⁵, Clonazepam⁵⁶ and famotidine⁵⁷. These transitions can be attributed to temperature-induced density changes in carbon dioxide and vapor pressure changes in solutes. The crossover pressure was investigated in several articles, which proposed some methods to predict the crossover pressure region^{58–60}. The crossover region varies depending on the critical properties of the solute, such as its sublimation pressure, sublimation enthalpy, partial molar enthalpy, and molar volume. Thus, the pressure range of 12–18 MPa was introduced as the crossover region for APZ drug (Fig. 2).

Semi-empirical models. Semi-empirical models such as Chrastil⁴⁹, Bartle et al.⁶¹, K-J⁶², MST⁶³, Sodeifian et al.³³, and Jouyban et al.⁶⁴ were used for the correlation of the solubility of APZ. Table 3 lists the equations of the semi-empirical models. Chrastil⁴⁹ proposed an equation for the solid solutes based on the SCF density and absolute temperature ($a_2 = \frac{\Delta H_t}{R}$), in which, the adjustable parameter of a_2 is a function of the total heat. R shows the global gas constant and ΔH_t represents the total heat of mixing. The vaporization enthalpy (ΔH_{vap}) can be determined by the model proposed by Bartle et al.⁶¹. According to the Hess' law, the solvation enthalpy (ΔH_{sol}) can be defined as the difference between ΔH_t and ΔH_{vap} . Sodeifian et al. proposed a semi-empirical model $a_0 - a_5$ and introduced six adjustable parameters. In 1998, K-J⁶² presented a density-based semi-empirical model for the correlation of the solid solubility in SCF. They expressed the relationship of a_2 with ΔH_t through $\Delta H_t = \frac{a_2}{R}$. A simple linear equation is shown by MST model for consistency of solid solubility in SCF.

Semi-empirical models of Chrastil⁴⁹, Sodeifian et al.³³, K-J⁶², MST⁶³, Bartle et al.³³, and Jouyban et al.⁶⁴ have three, six, three, three, three, and six parameters, respectively. The mentioned models were used from the Simulated Annealing algorithm for optimization. The adjustable parameters of the relevant statistical measures were obtained in terms of AARD% and R_{adj} for the CO₂-APZ binary system using the density-based models as listed in Table 4.

The average absolute relative deviation (AARD %) was used to assess the precision of the models:

Model	Formula
Chrastil ⁴⁹	$\ln s = a_0 \ln \rho + a_1 + \frac{a_2}{T}$
Bartle et al. ⁶¹	$\ln \frac{y_p}{\rho_{ref}} = a_0 + a_1(\rho - \rho_{ref}) + \frac{a_2}{T}$
K-J ⁶²	$\ln s = a_0 + a_1 \rho + \frac{a_2}{T}$
MST ⁶³	$\ln(Y_2P) = a_0 + a_1 \rho + a_2 T$
Sodeifian et al. ³³	$\ln y_2 = a_0 + (a_1 + a_2 \rho) \ln \rho + \frac{a_3}{T} + a_4 \ln(\rho T)$
Jouyban et al. ⁶⁴	$\ln y_2 = a_0 + a_1 \rho + a_2 P^2 + a_3 PT + \frac{a_4 T}{P} + a_5 \ln(\rho)$

Table 3. The semi-empirical models exploited in the present study.

Model	a_0	a_1	a_2	a_3	a_4	a_5	AARD%	R_{adj}
Chrastil ⁴⁹	4.8	-3608.9	-24	-	-	-	7.90	0.994
Bartle et al. ⁶¹	10.7	0.008	5861.49	-	-	-	10.73	0.971
KJ ⁶²	-4.5	0.2	3697.7	-	-	-	5.90	0.991
MST ⁶³	-8265.9	2.8	11.9	-	-	-	9.30	0.981
Sodeifian et al. ³³	179.73	-1.3	-17.225	0.017	-0.015	-8309.61	5.89	0.992
Jouyban et al. ⁶⁴	-20,722.88	2.093	-4.570	0.088	72.423	291.170	4.39	0.993

Table 4. Diverse parameters of APZ—CO₂ binary system, as obtained using models proposed by Chrastil, Bartle et al. Kumar and Johnston, MST, Sodeifian et al. and Jouyban et al.

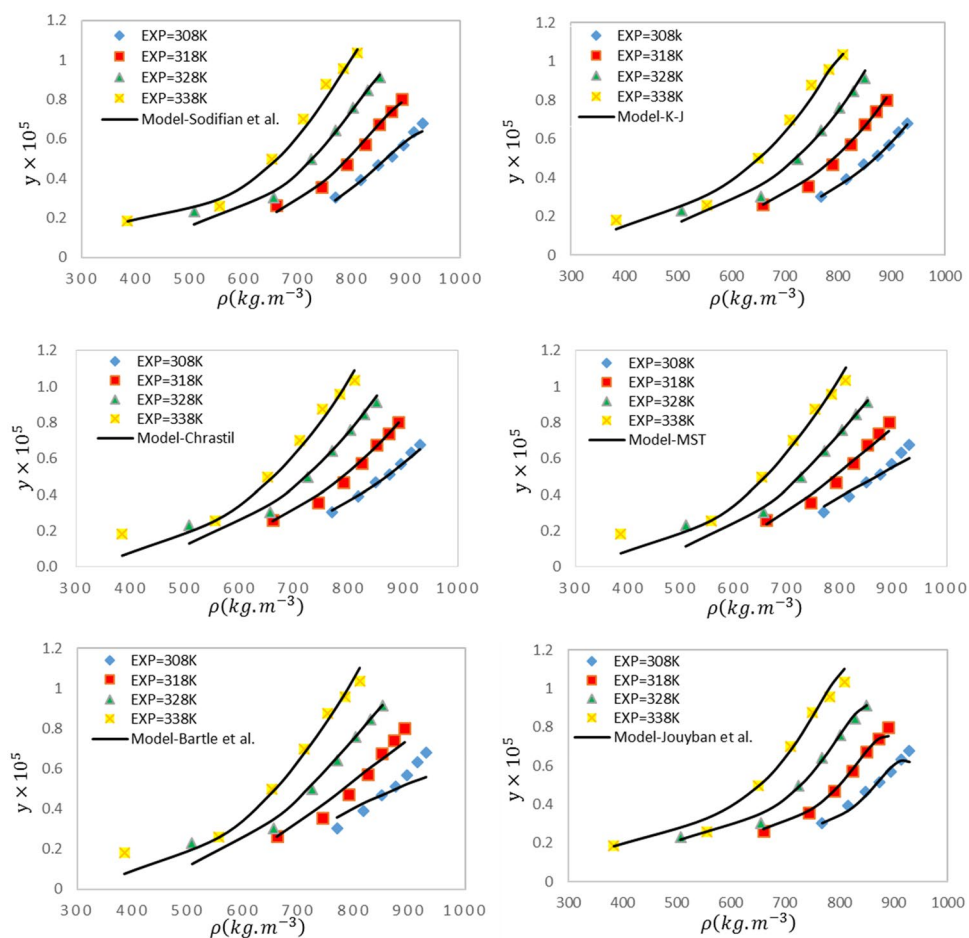


Figure 3. A comparison of experimental (points) and modeled (lines) values of APZ solubility based on semi-empirical models at different temperatures.

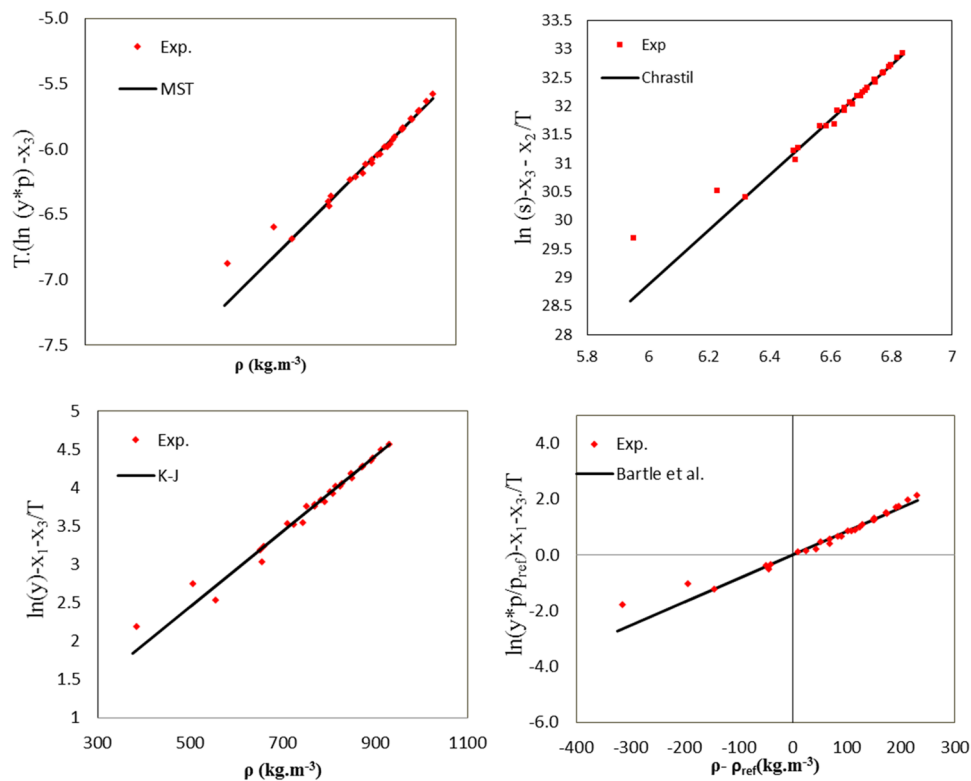


Figure 4. The self-consistency results obtained for four semi-empirical models. The lines suggest the linearity of the models.

$$AARD\% = \frac{100}{N_t - Z} \sum_{i=1}^{N_t} \frac{|y_2^{calc} - y_2^{exp}|}{y_2^{exp}} \quad (5)$$

In the above equation, Z represents the number of adjustable parameters of each model, N_t shows the number of data points in each set, and y_2 denotes the mole fraction solubility. The correlation coefficient adjusted by R_{adj} is defined as follows:

$$R_{adj} = \sqrt{|R^2 - (Q(1 - R^2)/(N - Q - 1))|} \quad (6)$$

While the correlation coefficient is represented by R^2 , the number of data points in each set is shown by N . Q also denotes the number of independent variables in each equation.

The AARD% values were 7.90, 10.73, 5.90, 9.30, 5.89, and 4.39 for Chrastil, Bartle et al., K-J, MST, Sodeifian et al., and Jouyban et al., respectively. The models proposed by Jouyban et al. and Sodeifian et al. showed the best performance in predicting the solubility of APZ with respective AARD% values of 4.39 and 5.89%. Jouyban et al. model exhibited the best correlation compared to others. The linear equation of Jouyban et al. is generally more suitable for predicting the solubility of this type of drug compared to the model proposed by Bartle et al. Other semi-empirical models offered acceptable predictive accuracies. The results also revealed the higher precision of the Chrastil model in predicting the solubility data with $R_{adj}=0.994$. Figure 3 compares the experimental solubility with those calculated by the density-based models.

Figure 4 demonstrates the self-consistency of experimental data of APZ solubility with Chrastil, Bartle et al., MST, and K-J models. The model is acceptable in self-consistency tests if all the solubility data obtained at different temperatures are located on the 45° degree line. The test results of the mentioned semi-empirical models suggest the consistency of the measured solubility values.

Table 5 lists the calculated enthalpy for APZ in SC-CO₂. The Chrastil model shows the approximate total heat of 30KJ.mol⁻¹. Based on Bartle's model, the enthalpy of vaporization was (48.73KJ.mol⁻¹). Solvation heat (ΔH_{sol}) was equal to 18.73KJ.mol⁻¹ based on the difference between ΔH_{vap} and ΔH_t .

Modified Wilson model. Since the solid solubility in the supercritical phase is very small, we can assume to be at infinite dilution condition. Consequently, the activity coefficient of the solid solute is the one at infinite dilution (γ_2^∞) and the density of the solution is that of the pure solvent. Therefore, the solubility equation is obtained:

Compound	$\Delta H_{\text{total}} \text{ (KJ.mol}^{-1}\text{)}^a$	$\Delta H_{\text{vap}} \text{ (KJ.mol}^{-1}\text{)}^b$	$\Delta H_{\text{sol}} \text{ (KJ.mol}^{-1}\text{)}^c$
APZ	30.00	48.73	-18.73

Table 5. The vaporization (ΔH_{vap}), approximated total (T_{total}), and solvation (ΔH_{sol}) enthalpy for APZ. ^aCalculated by the Chrastil's model⁴⁹. ^bCalculated by the Bartle et al. model³³. ^cCalculated by the difference between the ΔH_{vap} and ΔH_{total} .

A	B	λ_{12}	λ_{21}	AARD%	R_{adj}
-0.00000787	0.0000452	-2.78033	16.66676	6.82	0.985

Table 6. Modified Wilson model parameters for solubility of APZ in SC-CO₂.

$$y_2 = \frac{1}{\gamma_2^\infty} \exp \left[\frac{-\Delta H_2^f}{R} \left(\frac{1}{T} - \frac{1}{T_m} \right) \right] \quad (7)$$

$-\Delta H_2^f$ is the enthalpy of fusion and T_m is the melting point temperature of the solid solute.

Gibbs excess energy is defined according to the following formula for the binary system. Wilson's model has two variable parameters (λ_{12} and λ_{21}) which are the difference of intermolecular interaction energies of the molar volume of supercritical carbon dioxide. Moreover, ϑ_1 and ϑ_2 are dependent values due to the low solubility of the solute in the SC-CO₂ where ϑ_1 and ϑ_2 are the molar volumes of the SCF (expanded liquid) and the solid solute respectively. The following equation can be used to determine the activity coefficient:

$$\ln \gamma_2^\infty = 1 - \Lambda_{12} - \ln \Lambda_{21} \quad (8)$$

ϑ_1 and ϑ_2 can be defined under infinite dilution conditions:

$$\Lambda_{12} = \vartheta_2 \rho_{cl} \rho_r \exp \left(-\frac{\lambda'_{12}}{T_r} \right) \quad (9)$$

$$\Lambda_{21} = \frac{1}{\vartheta_2 \rho_{cl} \rho_r} \exp \left(-\frac{\lambda'_{21}}{T_r} \right) \quad (10)$$

ρ_r is the reduced density of the solvent (SCF) equal to ρ / ρ_{cl} , where ρ_{cl} is its critical density and the dimensionless energies of interaction are as follow:

$$\lambda_{12} = \frac{\lambda'_{12}}{RT_{C1}} \quad (11)$$

$$\lambda_{21} = \frac{\lambda'_{21}}{RT_{C1}} \quad (12)$$

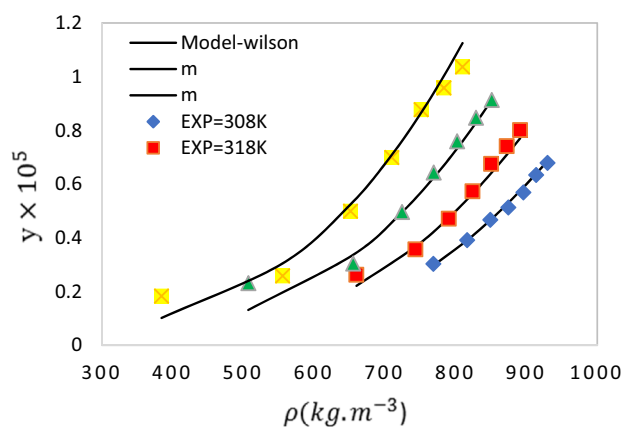


Figure 5. Experimental data (point) and calculated (line) solubility of APZ in SC-CO₂ based on the modified Wilson model.

A linear equation can be defined between molar volume and reduced density to capture the effect of high pressure on the model:

$$\vartheta_2 = \alpha\rho_r + \beta \quad (13)$$

λ_{12} , λ_{21} , α , and β were obtained by the model.

Using the extended liquid theory, the modified Wilson model was utilized for optimization of the parameters of the model of APZ solubility in SC-CO₂. Table 6 summarizes the parameters of the modified Wilson model (α , β , λ_{12} , λ_{21}). A comparison of experimental and modeled data (Fig. 5) confirmed the accuracy of the modified Wilson model. Based on Table 6, λ_{21} is smaller than λ_{12} as also reported in previous studies^{27,34,50,51,65}.

Conclusion

APZ solubility was evaluated at different pressures (12, 15, 18, 21, 24, 27, and 30 MPa) and temperatures (308, 318, 328, and 338 K). The molar fraction of APZ in SC-CO₂ varied from 1.83×10^{-6} to 1.036×10^{-5} . The lowest and highest molar fractions of APZ were detected at a constant temperature of 338 K and pressures of 12 and 30 MPa, respectively. Six semi-empirical models (Sodeifian et al., Jouyban et al., Chrastil, Bartle et al., MST, K-J), and an extended liquid theory (modified Wilson model) were employed for the correlation of the experimental solubility data. The precision of the models was explored in terms of AARD% and R_{adj} . Accordingly, the modified Wilson model (AARD% = 6.82) and the semi-empirical models of Chrastil (AARD% = 7.90), Bartle et al. (AARD% = 10.73), Jouyban (AARD% = 4.39), MST (AARD% = 9.30), Kumar Johnston (AARD% = 5.90), Sodeifian et al. (AARD% = 5.89), Jouyban et al., and Sodeifian et al. with six adjustable parameters showed the best correlation among density-based models, reflecting the ability of this model to correlate solubility data. Such satisfactory correlation results of the semi-empirical models also show the self-consistency of the experimental findings. The models of Chrastil and Bartle et al. were also applied to determine the enthalpy of vaporization and solvation.

Data availability

The datasets used and/or analyzed during the current study are available upon reasonable request from the corresponding author.

Received: 16 April 2023; Accepted: 12 August 2023

Published online: 17 August 2023

References

- Harrison, T. S. & Perry, C. M. Aripiprazole: A review of its use in schizophrenia and schizoaffective disorder. *Drugs* **64**, 1715–1736. <https://doi.org/10.2165/00003495-200464150-00010> (2004).
- Jalles, A. et al. Aripiprazole offsets mutant ATXN3-Induced motor dysfunction by targeting dopamine D2 and serotonin 1A and 2A receptors in *C. elegans*. *Biomedicine* **10**, 370. <https://doi.org/10.3390/biomedicine10020370> (2022).
- Kishi, T. et al. Mood stabilizers and/or antipsychotics for bipolar disorder in the maintenance phase: A systematic review and network meta-analysis of randomized controlled trials. *Mol. Psychiatry* **26**, 4146–4157. <https://doi.org/10.1038/s41380-020-00946-6> (2021).
- Cantù, F. et al. Augmentation with atypical antipsychotics for treatment-resistant depression. *J. Affect. Disord.* **280**, 45–53. <https://doi.org/10.1016/j.jad.2020.11.006> (2021).
- Badr-Eldin, S. M., Ahmed, T. A. & Ismail, H. R. Aripiprazole-cyclodextrin binary systems for dissolution enhancement: Effect of preparation technique, cyclodextrin type and molar ratio. *Iran. J. Basic Med. Sci.* **16**, 1223 (2013).
- Burris, K. D. et al. Aripiprazole, a novel antipsychotic, is a high-affinity partial agonist at human dopamine D2 receptors. *J. Pharmacol. Exp. Ther.* **302**, 381–389. <https://doi.org/10.1124/jpet.102.033175> (2002).
- Sawant, K., Pandey, A. & Patel, S. Aripiprazole loaded poly (caprolactone) nanoparticles: Optimization and in vivo pharmacokinetics. *Mater. Sci. Eng. C* **66**, 230–243. <https://doi.org/10.1016/j.msec.2016.04.089> (2016).
- Chen, L.-F. et al. Preparation of aripiprazole-poly (methyl vinyl ether-co-maleic anhydride) nanocomposites via supercritical antisolvent process for improved antidepressant therapy. *Regen. Biomater.* <https://doi.org/10.1093/rb/rbac080> (2022).
- Seki, Y. et al. Pretreatment of aripiprazole and minocycline, but not haloperidol, suppresses oligodendrocyte damage from interferon- γ -stimulated microglia in co-culture model. *Schizophr. Res.* **151**, 20–28. <https://doi.org/10.1016/j.schres.2013.09.011> (2013).
- Stapel, B. et al. Second generation atypical antipsychotics olanzapine and aripiprazole reduce expression and secretion of inflammatory cytokines in human immune cells. *J. Psychiatr. Res.* **105**, 95–102. <https://doi.org/10.1016/j.jpsychires.2018.08.017> (2018).
- McFall, H. et al. Formulation of aripiprazole-loaded pH-modulated solid dispersions via hot-melt extrusion technology: In vitro and in vivo studies. *Int. J. Pharm.* **554**, 302–311. <https://doi.org/10.1016/j.ijpharm.2018.11.005> (2019).
- Prasanthi, D. et al. Formulation and evaluation of aripiprazole oral disintegrating tablets. *J. Pharm. Res. Int.* <https://doi.org/10.9734/jpri/2022/v34i49b36429> (2022).
- Esfandiari, N. & Sajadian, S. A. Experimental and modeling investigation of Glibenclamide solubility in supercritical carbon dioxide. *Fluid Phase Equilib.* **556**, 113408. <https://doi.org/10.1016/j.fluid.2022.113408> (2022).
- Sodeifian, G., Ardestani, N. S., Sajadian, S. A. & Panah, H. S. Experimental measurements and thermodynamic modeling of Coumarin-7 solid solubility in supercritical carbon dioxide: Production of nanoparticles via RESS method. *Fluid Phase Equilib.* **483**, 122–143. <https://doi.org/10.1016/j.fluid.2018.11.006> (2019).
- Sodeifian, G., Sajadian, S. A., Ardestani, N. S. & Razmimanesh, F. Production of Loratadine drug nanoparticles using ultrasonic-assisted Rapid expansion of supercritical solution into aqueous solution (US-RESSAS). *J. Supercrit. Fluids* **147**, 241–253. <https://doi.org/10.1016/j.supflu.2018.11.007> (2019).
- Razmimanesh, F., Sodeifian, G. & Sajadian, S. A. An investigation into Sunitinib malate nanoparticle production by US-RESOLV method: Effect of type of polymer on dissolution rate and particle size distribution. *J. Supercrit. Fluids* **170**, 105163. <https://doi.org/10.1016/j.supflu.2021.105163> (2021).
- Esfandiari, N. & Ghoreishi, S. M. Optimal thermodynamic conditions for ternary system (CO₂, DMSO, ampicillin) in supercritical CO₂ antisolvent process. *J. Taiwan Inst. Chem. Eng.* **50**, 31–36. <https://doi.org/10.1016/j.jtice.2014.12.015> (2015).
- Esfandiari, N. & Ghoreishi, S. M. Ampicillin nanoparticles production via supercritical CO₂ gas antisolvent process. *AAPS Pharm-SciTech* **16**, 1263–1269. <https://doi.org/10.1208/s12249-014-0264-y> (2015).

19. Najafi, M., Esfandiari, N., Honarvar, B. & Aboosadi, Z. A. Experimental investigation on finasteride microparticles formation via gas antisolvent process. *J. Kiss*. **59**, 455–466 (2021).
20. Najafi, M., Esfandiari, N., Honarvar, B. & Aboosadi, Z. A. Production of Rosuvastatin calcium nanoparticles using gas antisolvent technique: Experimental and optimization. *Periodica Polytech. Chem. Eng.* **65**, 442–453. <https://doi.org/10.3311/ppch.16629> (2021).
21. Esfandiari, N. & Ghoreishi, S. M. Synthesis of 5-fluorouracil nanoparticles via supercritical gas antisolvent process. *J. Supercrit. Fluids* **84**, 205–210. <https://doi.org/10.1016/j.supflu.2013.10.008> (2013).
22. Vorobei, A. & Parenago, O. Using supercritical fluid technologies to prepare micro- and nanoparticles. *Russ. J. Phys. Chem. A* **95**, 407–417. <https://doi.org/10.1134/s0036024421030237> (2021).
23. Sodeifian, G., Hsieh, C.-M., Derakhsheshpour, R., Chen, Y.-M. & Razmimanesh, F. Measurement and modeling of metoclopramide hydrochloride (anti-emetic drug) solubility in supercritical carbon dioxide. *Arab. J. Chem.* **15**, 103876. <https://doi.org/10.1016/j.arabjc.2022.103876> (2022).
24. Sodeifian, G. & Sajadian, S. A. Utilization of ultrasonic-assisted RESOLV (US-RESOLV) with polymeric stabilizers for production of amidarone hydrochloride nanoparticles: Optimization of the process parameters. *Chem. Eng. Res. Des.* **142**, 268–284. <https://doi.org/10.1016/j.cherd.2018.12.020> (2019).
25. Sodeifian, G., Nasri, L., Razmimanesh, F. & Abadian, M. Measuring and modeling the solubility of an antihypertensive drug (losartan potassium, Cozaar) in supercritical carbon dioxide. *J. Mol. Liquids* **331**, 115745. <https://doi.org/10.1016/j.molliq.2021.115745> (2021).
26. Sodeifian, G., Alwi, R. S., Razmimanesh, F. & Tamura, K. Solubility of quetiapine hemifumarate (antipsychotic drug) in supercritical carbon dioxide: Experimental, modeling and hansen solubility parameter application. *Fluid Phase Equilib.* **537**, 113003. <https://doi.org/10.1016/j.fluid.2021.113003> (2021).
27. Sajadian, S. A., Amani, M., Ardestani, N. S. & Shirazian, S. Experimental analysis and thermodynamic modelling of lenalidomide solubility in supercritical carbon dioxide. *Arab. J. Chem.* **15**, 103821. <https://doi.org/10.1016/j.arabjc.2022.103821> (2022).
28. Amani, M., Ardestani, N. S. & Majid, N. Y. Utilization of supercritical CO₂ gas antisolvent (GAS) for production of Capecitabine nanoparticles as anti-cancer drug: Analysis and optimization of the process conditions. *J. CO₂ Util.* **46**, 101465. <https://doi.org/10.1016/j.jcou.2021.101465> (2021).
29. Cocero, M. J., Martín, Á., Mattea, F. & Varona, S. Encapsulation and co-precipitation processes with supercritical fluids: Fundamentals and applications. *J. Supercrit. Fluids* **47**, 546–555. <https://doi.org/10.1016/j.supflu.2008.08.015> (2009).
30. Martín, A. & Cocero, M. J. Micronization processes with supercritical fluids: Fundamentals and mechanisms. *Adv. Drug Deliv. Rev.* **60**, 339–350. <https://doi.org/10.1016/j.addr.2007.06.019> (2008).
31. Reverchon, E., Adami, R., Cardea, S. & Della Porta, G. Supercritical fluids processing of polymers for pharmaceutical and medical applications. *J. Supercrit. Fluids* **47**, 484–492. <https://doi.org/10.1016/j.supflu.2008.10.001> (2009).
32. Padrela, L. *et al.* Supercritical carbon dioxide-based technologies for the production of drug nanoparticles/nanocrystals—A comprehensive review. *Adv. Drug Deliv. Rev.* **131**, 22–78. <https://doi.org/10.1016/j.addr.2018.07.010> (2018).
33. Sodeifian, G., Razmimanesh, F. & Sajadian, S. A. Solubility measurement of a chemotherapeutic agent (Imatinib mesylate) in supercritical carbon dioxide: Assessment of new empirical model. *J. Supercrit. Fluids* **146**, 89–99. <https://doi.org/10.1016/j.supflu.2019.01.006> (2019).
34. Sodeifian, G., Ardestani, N. S., Razmimanesh, F. & Sajadian, S. A. Experimental and thermodynamic analyses of supercritical CO₂-Solubility of minoxidil as an antihypertensive drug. *Fluid Phase Equilib.* **522**, 112745. <https://doi.org/10.1016/j.fluid.2020.112745> (2020).
35. Zabihi, S. *et al.* Measuring salsalate solubility in supercritical carbon dioxide: Experimental and thermodynamic modelling. *J. Chem. Thermodyn.* **152**, 106271. <https://doi.org/10.1016/j.jct.2020.106271> (2021).
36. Schmitt, W. J. & Reid, R. C. Solubility of monofunctional organic solids in chemically diverse supercritical fluids. *J. Chem. Eng. Data* **31**, 204–212. <https://doi.org/10.1021/je00044a021> (1986).
37. Kosal, E. & Holder, G. D. Solubility of anthracene and phenanthrene mixtures in supercritical carbon dioxide. *J. Chem. Eng. Data* **32**, 148–150. <https://doi.org/10.1021/je00048a005> (1987).
38. Aionicesei, E., Škerget, M. & Knez, Ž. Measurement of CO₂ solubility and diffusivity in poly (l-lactide) and poly (d, l-lactide-co-glycolide) by magnetic suspension balance. *J. Supercrit. Fluids* **47**, 296–301. <https://doi.org/10.1016/j.supflu.2008.07.011> (2008).
39. Dobbs, J., Wong, J., Lahiere, R. & Johnston, K. Modification of supercritical fluid phase behavior using polar cosolvents. *Ind. Eng. Chem. Res.* **26**, 56–65. <https://doi.org/10.1021/ie00061a011> (1987).
40. Yamini, Y., Fat'hi, M. R., Alizadeh, N. & Shamsipur, M. Solubility of dihydroxybenzene isomers in supercritical carbon dioxide. *Fluid Phase Equilib.* **152**, 299–305. [https://doi.org/10.1016/s0378-3812\(98\)00385-9](https://doi.org/10.1016/s0378-3812(98)00385-9) (1998).
41. Keshmiri, K., Vatanara, A. & Yamini, Y. Development and evaluation of a new semi-empirical model for correlation of drug solubility in supercritical CO₂. *Fluid Phase Equilib.* **363**, 18–26. <https://doi.org/10.1016/j.fluid.2013.11.013> (2014).
42. Asiabi, H., Yamini, Y., Latifeh, F. & Vatanara, A. Solubilities of four macrolide antibiotics in supercritical carbon dioxide and their correlations using semi-empirical models. *J. Supercrit. Fluids* **104**, 62–69. <https://doi.org/10.1016/j.supflu.2015.05.018> (2015).
43. Johannsen, M. & Brunner, G. Solubilities of the fat-soluble vitamins A, D, E, and K in supercritical carbon dioxide. *J. Chem. Eng. Data* **42**, 106–111. <https://doi.org/10.1021/je960219m> (1997).
44. Stahl, E., Schilz, W., Schütz, E. & Willing, E. A quick method for the microanalytical evaluation of the dissolving power of supercritical gases. *Angew. Chem. Int. Ed. Engl.* **17**, 731–738. <https://doi.org/10.1002/anie.197807311> (1978).
45. Anvari, M. H. & Pazuki, G. A study on the predictive capability of the SAFT-VR equation of state for solubility of solids in supercritical CO₂. *J. Supercrit. Fluids* **90**, 73–83. <https://doi.org/10.1016/j.supflu.2014.03.005> (2014).
46. Sodeifian, G., Sajadian, S. A. & Derakhsheshpour, R. Experimental measurement and thermodynamic modeling of Lansoprazole solubility in supercritical carbon dioxide: Application of SAFT-VR EoS. *Fluid Phase Equilib.* **507**, 112422. <https://doi.org/10.1016/j.fluid.2019.112422> (2020).
47. Taberero, A., De Melo, S. V., Mammucari, R., Del Valle, E. M. & Foster, N. Modelling solubility of solid active principle ingredients in sc-CO₂ with and without cosolvents: A comparative assessment of semiempirical models based on Chrastil's equation and its modifications. *J. Supercrit. Fluids* **93**, 91–102. <https://doi.org/10.1016/j.fluid.2019.112422> (2014).
48. Amani, M., Ardestani, N. S., Jouyban, A. & Sajadian, S. A. Solubility measurement of the fludrocortisone acetate in supercritical carbon dioxide: Experimental and modeling assessments. *J. Supercrit. Fluids* **190**, 105752. <https://doi.org/10.1016/j.supflu.2022.105752> (2022).
49. Chrastil, J. Solubility of solids and liquids in supercritical gases. *J. Phys. Chem.* **86**, 3016–3021. <https://doi.org/10.1021/j100212a041> (1982).
50. Esfandiari, N. & Sajadian, S. A. Solubility of Lacosamide in supercritical carbon Dioxide: An experimental analysis and thermodynamic modeling. *J. Mol. Liquids* **360**, 119467. <https://doi.org/10.1016/j.molliq.2022.119467> (2022).
51. Nasri, L. Modified Wilson's model for correlating solubilities in supercritical fluids of some polycyclic aromatic solutes. *Polycyclic Aromat. Compd.* **38**, 244–256. <https://doi.org/10.1080/10406638.2016.1200636> (2018).
52. Morales-Díaz, C., Cabrera, A. L., Juan, C. & Mejía, A. Modelling of solubility of vitamin K3 derivatives in supercritical carbon dioxide using cubic and SAFT equations of state. *J. Supercrit. Fluids* **167**, 105040. <https://doi.org/10.1016/j.supflu.2020.105040> (2021).
53. Poling, B. E., Prausnitz, J. M. & O'connell, J. P. *Properties of Gases and Liquids* (McGraw-Hill Education, 2001). <https://doi.org/10.1016/j.supflu.2020.105040>.

54. Immirzi, A. & Perini, B. Prediction of density in organic crystals. *Acta Crystallogr. Sect. A* **33**, 216–218. <https://doi.org/10.1107/s0567739477000448> (1977).
55. Sajadian, S. A., Peyrovedin, H., Zomorodian, K. & Khorram, M. Using the supercritical carbon dioxide as the solvent of Nystatin: Studying the effect of co-solvent, experimental and correlating. *J. Supercrit. Fluids* **194**, 105858. <https://doi.org/10.1016/j.supflu.2023.105858> (2023).
56. Alwi, R. S. *et al.* Experimental study and thermodynamic modeling of clonazepam solubility in supercritical carbon dioxide. *Fluid Phase Equilib.* <https://doi.org/10.1016/j.fluid.2023.113880> (2023).
57. Ardestani, N. S., Sajadian, S. A., Rojas, A., Alwi, R. & Estévez, L. A. Solubility of famotidine in supercritical carbon dioxide: Experimental measurement and thermodynamic modeling. *J. Supercrit. Fluids* <https://doi.org/10.1016/j.supflu.2023.106031> (2023).
58. de Melo, S. V., Costa, G. M. N., Viana, A. & Pessoa, F. Solid pure component property effects on modeling upper crossover pressure for supercritical fluid process synthesis: A case study for the separation of Annatto pigments using SC-CO₂. *J. Supercrit. Fluids* **49**, 1–8. <https://doi.org/10.1016/j.supflu.2008.12.006> (2009).
59. Kalikin, N. *et al.* Carbamazepine solubility in supercritical CO₂: A comprehensive study. *J. Mol. Liquids* **311**, 113104. <https://doi.org/10.1016/j.molliq.2020.113104> (2020).
60. Kalikin, N., Oparin, R., Kolesnikov, A., Budkov, Y. & Kiselev, M. A crossover of the solid substances solubility in supercritical fluids: What is it in fact?. *J. Mol. Liquids* **334**, 115997. <https://doi.org/10.1016/j.molliq.2021.115997> (2021).
61. Bartle, K., Clifford, A., Jafar, S. & Shilstone, G. Solubilities of solids and liquids of low volatility in supercritical carbon dioxide. *J. Phys. Chem. Ref. Data* **20**, 713–756. <https://doi.org/10.1063/1.555893> (1991).
62. Kumar, S. K. & Johnston, K. P. Modelling the solubility of solids in supercritical fluids with density as the independent variable. *J. Supercrit. Fluids* **1**, 15–22. [https://doi.org/10.1016/0896-8446\(88\)90005-8](https://doi.org/10.1016/0896-8446(88)90005-8) (1988).
63. Méndez-Santiago, J. & Teja, A. S. The solubility of solids in supercritical fluids. *Fluid Phase Equilib.* **158**, 501–510. [https://doi.org/10.1016/S0378-3812\(99\)00154-5](https://doi.org/10.1016/S0378-3812(99)00154-5) (1999).
64. Jouyban, A. *et al.* Solubility prediction in supercritical CO₂ using minimum number of experiments. *J. Pharm. Sci.* **91**, 1287–1295. <https://doi.org/10.1002/jps.10127> (2002).
65. Sodeifian, G., Ardestani, N. S. & Sajadian, S. A. Solubility measurement of a pigment (Phthalocyanine green) in supercritical carbon dioxide: Experimental correlations and thermodynamic modeling. *Fluid Phase Equilib.* **494**, 61–73. <https://doi.org/10.1016/j.fluid.2019.04.024> (2019).

Author contributions

E.A.: Methodology, Writing- Original draft preparation, Data curation, Software. B.H.: Conceptualization, Investigation, Validation, funding acquisition, reviewing and Editing. S.A.S.: Conceptualization, project administration, Software, supervision, reviewing and editing. M.A.A.: validation, Methodology, writing, validation, visualization, reviewing. Z.A.A.: Investigation, methodology, validation, review and writing. All authors reviewed the manuscript.

Competing interests

The authors declare no competing interests.

Additional information

Correspondence and requests for materials should be addressed to B.H.

Reprints and permissions information is available at www.nature.com/reprints.

Publisher's note Springer Nature remains neutral with regard to jurisdictional claims in published maps and institutional affiliations.



Open Access This article is licensed under a Creative Commons Attribution 4.0 International License, which permits use, sharing, adaptation, distribution and reproduction in any medium or format, as long as you give appropriate credit to the original author(s) and the source, provide a link to the Creative Commons licence, and indicate if changes were made. The images or other third party material in this article are included in the article's Creative Commons licence, unless indicated otherwise in a credit line to the material. If material is not included in the article's Creative Commons licence and your intended use is not permitted by statutory regulation or exceeds the permitted use, you will need to obtain permission directly from the copyright holder. To view a copy of this licence, visit <http://creativecommons.org/licenses/by/4.0/>.

© The Author(s) 2023